ACS APPLIED ENERGY MATERIALS

www.acsaem.org Article

Enhanced Thermoelectric Performance in Polypyrrole-Based Multilayer Nanoarchitectures via Thermal Reduction

Mario Culebras,*,○ You-young Byun,○ Junho Jang, Tae Kwon Lee, Dongwhi Choi, Aleksandra Serafin, Maurice N. Collins, Jung Sang Cho,* and Chungyeon Cho*

Cite This: *ACS Appl. Energy Mater.* 2024, 7, 2351−2361 Read Online

ACCESS | Metrics & More | Article Recommendations | Supporting Information

ABSTRACT: In this study, cationic polypyrrole nanoparticles (PPy:NPs) are synthesized in a water-based solution in order to serve as a template that facilitates the formation of flexible hierarchical structures, ultimately resulting in improved thermoelectric (TE) performance. A unique multilayered structure is fabricated by alternately depositing positively charged PPy:NPs and negatively charged double-walled carbon nanotube-graphene oxide (DWNT-GO) suspensions via layer-by-layer deposition. The resulting polymer/carbon composite, consisting of a 16-bilayer PPy:NPs/DWNT-GO with a thickness of approximately 2.45 μm, exhibited an electrical conductivity of 1.36 S/cm and a Seebeck coefficient of 84 μV/K, yielding a power factor of 0.96 μW/m·K^2. A thermal reduction process at 175 °C for 90 min significantly enhanced the electrical conductivity (183.2 S/cm) and Seebeck coefficient (115 μV/K), resulting in a remarkable power factor of 242.2 μW/m·K^2. This is one of the highest values ever reported for PPy-based organic TE materials. The outstanding TE properties can be attributed to the creation of a highly organized three-dimensional conjugated network after thermal reduction, which promotes carrier transport within the multilayers.

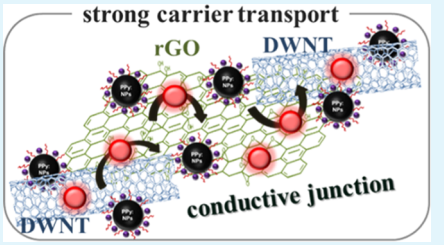

KEYWORDS: *polypyrrole, layer-by-layer assembly, graphene oxide, thermoelectric power factor, carbon nanotubes*

1. INTRODUCTION

With the progress of the high-tech industries, the demand for small electronic and wearable devices has surged, leading to a significant increase in energy consumption. According to the U.S. Energy Information Administration, there will be a 56% increase in energy consumption to 820 quadrillioin Btu in by 2040 from 524 quadrillion Btu in 2010.[1] Given the environmental impact and global warming effects of conventional energy sources such as petroleum and coal, extensive research has focused on the development of sustainable and clean energy alternatives. Energy-harvesting technologies such as piezoelectric, tidal, hydro, and triboelectric materials have emerged as renewable substitutes for fossil fuels.[2−4] These functional materials have been developed to address the increasing energy demands and associated challenges posed by conventional energy sources. Specifically, thermoelectric (TE) material-based power generation technologies have been recognized as a reliable and promising strategy to harness low-grade waste heat in an eco-friendly manner. This is because these technologies entail no moving parts and require no hazardous gases or working fluids.[5−7] Furthermore, their low maintenance requirements and long operational lifespans render them cost-effective and sustainable in the long run.[8] TE materials can directly convert waste heat to electricity wherever a temperature gradient exists. TE conversion efficiency relies on a dimensionless figure of merit (ZT): $ZT = S^2 \cdot \sigma \cdot T/\kappa$, where S, σ, κ, and T are the Seebeck coefficient, electrical conductivity, thermal conductivity, and absolute temperature, respectively. Thus, high-efficiency TE devices should possess large S, σ, and low κ values. Due to the difficulty in precisely measuring κ values of thin films and intrinsically low κ, the power factor ($PF = S^2 \cdot \sigma$) is usually analyzed in polymer-based organic materials.[9−14]

Inorganic nanostructures, including Bi_2Te_3, Bi_2Se_3, PbTe, $CoSb_3$, and semiconductor alloys (e.g., PbSeTe and SiGe), have been reported to exhibit remarkable efficiency in converting heat into useful electricity, achieving ZT values greater than 1. However, these materials require high-temperature and complicated processes to achieve high TE performances. Inorganic materials-based TE generators often suffer from poor mechanical flexibility and are also associated with toxicity and high production costs. These issues hinder their wide practical application in wearable devices.[15] Recently, conjugated semiconducting polymers have been considered as promising materials for TE applications due to their unique features, such as abundance of starting materials, easy processability, and tunable electrical conductivity.[16−18] Other

Received: December 12, 2023
Revised: February 25, 2024
Accepted: February 26, 2024
Published: March 11, 2024

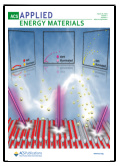

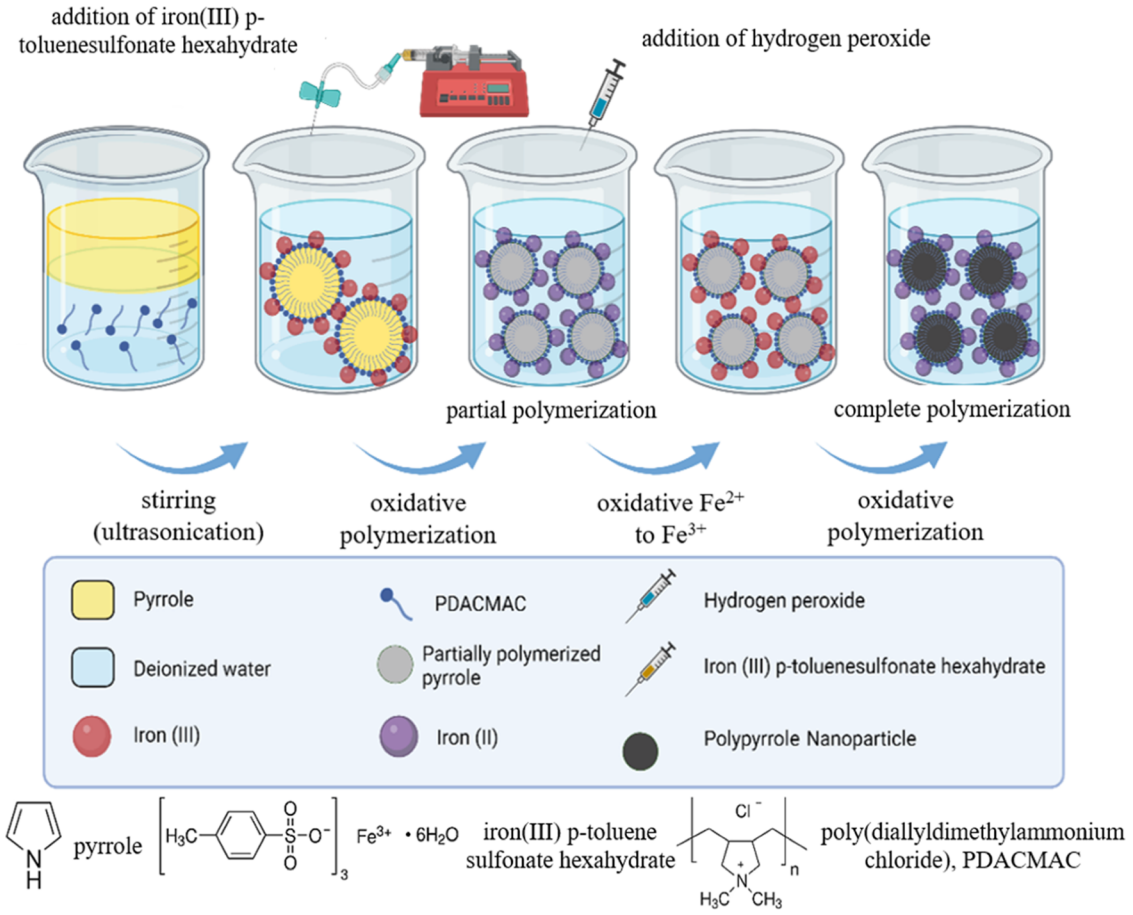

Figure 1. Synthesis process of polypyrrole nanoparticles.

advantages include the ease of processing into complex configurations and intrinsically low k (within 0.1−0.9 W/m·K) as compared to crystalline inorganic materials, which is beneficial for achieving high ZT values.[19,20] Commonly used polymers for TE organics have been limited to intrinsically conductive polymers, including polyaniline, poly(3,4-ethylenedioxythiophene):poly(styrenesulfonate), polypyrrole (PPy), and polythiophene.[21−24] In particular, cationic water-soluble conjugated polymers are scarce because of the challenges associated with their synthesis. Therefore, the development of conductive polymers with exceptional TE behavior is essential for expanding the application of organic TE materials across diverse industrial applications spanning structural components to electronic devices.

Substantial efforts to fabricate organic composites with enhanced TE performances have been reported; to this end, various approaches, including in situ polymerization, physical mixing, melt mixing, electrochemical polymerization, and interfacial polymerization, have been employed.[25−28] Organic composites based on these methods have shown reasonably good TE properties. However, there is a growing demand for a coating strategy that enhances the electrical conductivity and Seebeck coefficient while retaining the advantages of the individual components (such as carbon materials and intrinsically conductive polymers) of the composites. In this regard, layer-by-layer (LbL) assembly has been recognized one of the most efficient approach due to its high degree of control in film's architecture and property, which otherwise could not be realized simply by combining organic materials.[29] The LbL approach is a versatile but powerful method to create nanoscaled multifunctional thin films by utilizing electrostatic interaction, hydrogen bonding, and covalent bonding between molecules, regardless of the substrate shape.[30−32] It has also become increasingly popular in various applications including the creation of flexible displays, transparent electrodes, gas barriers, and flame retardants.[33−36] This self-assembly technique enables precise control over the nanostructure and properties of the films by adjusting various parameters such as deposition cycles, molecular weight, temperature, chemistry, assembly pH solutions, and ionic strength.[37−41] Such fine-tuning has been demonstrated to develop polymer nanocomposites that exhibit superior performance compared to the individual components and bulk films composed of the same materials.[42] Significant advancements have been achieved in the field of organic TE materials by synergistically incorporating conducting polymers and carbonaceous nanofillers (*e.g.*, graphene, graphene oxide (GO), and carbon nanotubes).[43−45]

This study demonstrates the synthesis of positively charged PPy nanoparticles (PPy:NPs) with high water solubility and the application of the LbL method for their assembly with GO-stabilized double-walled carbon nanotubes (DWNTs). A thin film composed of 16 layers of PPy:NPs/DWNT-GO with a thickness of approximately 2.45 μm was found to exhibit a low electrical conductivity of 1.36 S/cm and a Seebeck coefficient of 84 μV/K, resulting in a relatively low PF of 0.96 μW/m·K^2. However, upon subjecting this GO-based film to a 90 min heat treatment at 175 °C, the electrical conductivity and Seebeck coefficient significantly improved, reaching up to 183.2 S/cm

https://doi.org/10.1021/acsaem.3c03060
ACS Appl. Energy Mater. 2024, 7, 2351−2361

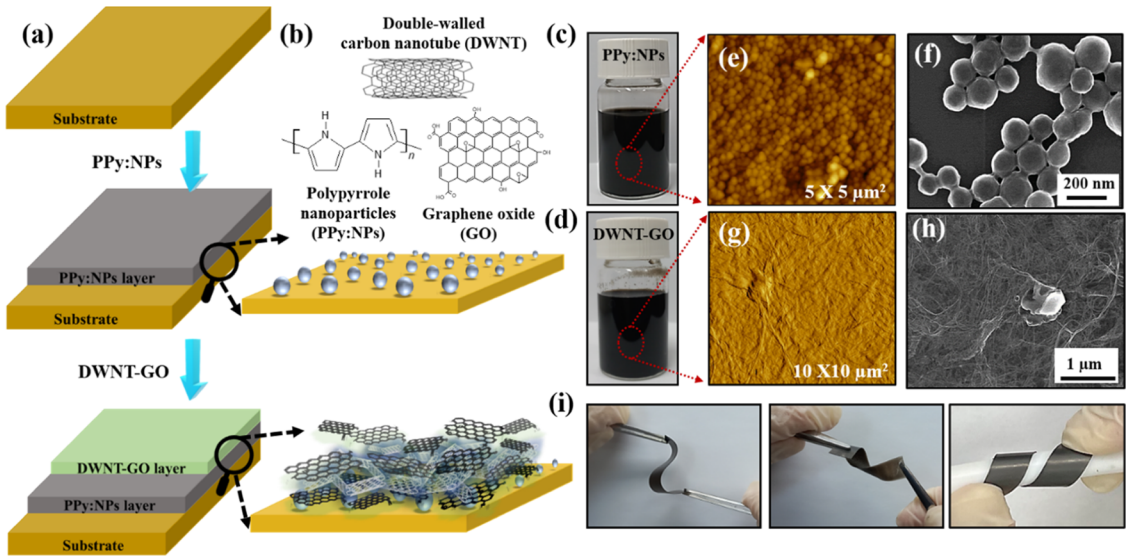

Figure 2. (a) Schematic diagram of a multilayered PPy:NPs/DWNT-GO coating via layer-by-layer deposition. (b) Molecular structures used in this study. Optical images of (c) PPy:NPs in water and (d) DWNT, stabilized in GO solution, and corresponding AFM (e, g) and SEM images (f, h) next to each vial. (i) Photo images of 16 BL PPy:NPs/DWNT-GO thin films coated on PET substrates upon bending (left), twisting (middle), and rolling (right).

and 115 μV/K, respectively. This translated to a remarkable PF of 242.2 μW/m·K^2, which is one of the highest power factors ever reported for PPy-based organic TE materials. These enhancements in the TE behavior can be attributed to the increased carrier mobility, which results from the extensively conjugated network created by the low-temperature treatment. The three-dimensional (3D) expanded architecture facilitates more efficient carrier transport in multilayer structures, thereby boosting the TE performance.

2. EXPERIMENTAL SECTION

2.1. Materials. Ultrahighly concentrated aqueous GO solution was purchased from Graphene Supermarket (Graphene Laboratories Inc., NY). DWNT (purity: ≥95%, length: 1 μm, and outside diameter: ∼3 nm) was obtained from Continental Carbon Nanotechnology Inc. (Huston, TX). A homogeneously dispersed suspension was achieved by subjecting DWNT (0.02 wt %)−GO (0.2 wt %) mixtures to a 30 min tip sonication at 40 W in an ice bath, followed by 20 min of bath sonication. All aqueous solutions were prepared from a Milli-Q water purification system with a resistivity of 18.2 MΩ·cm at 25 °C. Solutions were used without alteration of the pH. PPy:NPs were synthesized via chemical oxidation polymerization in a mini-emulsion, as depicted in Figure 1. First, 200 μL of pyrrole (0.037 M) was introduced into a 40 mL aqueous solution of poly(diallyldimethylammonium chloride). Thereafter, the mixture was subjected to stirring at 800 rpm for 5 min, followed by 10 min of tip ultrasonication by using a Soniprep 150 Plus (MSE, U.K.) on ice with an amplitude of 20 μm. This process resulted in the formation of a mini-emulsion. Subsequently, a 10 mL solution of Fe-Tos (0.056 M) in deionized (DI) water was gradually added to the mini-emulsion under constant stirring at 45 °C. Then, H_2O_2 (0.001 M) was introduced, and the reaction was allowed to proceed overnight. To purify the NPs, centrifugation was performed at 8700 rpm for 20 min. The supernatant was removed, and this purification step was carried out three times, ultimately resulting in the final redispersion of the NPs in 40 mL of DI water.

2.2. Substrates. Poly(ethylene terephthalate) (PET) was obtained from FilmBank (Gyeonggi-do, Korea) and used for conducting thermoelectric property analysis. Before the LbL coating process, the PET film was rinsed with methanol and DI water. Subsequently, the cleaned PET substrate was dried using an air gun, and a corona treater (BD-20C, Chicago, IL) was used to induce a negative charge on the PET surface, thereby enhancing the adhesion of the first PPy:NPs layer. For analytical characterizations such as profilometer, atomic force microscopy (AFM), scanning electron microscopy (SEM), Raman spectroscopy, X-ray photoelectron spectroscopy (XPS), and ultraviolet photoelectron spectroscopy (UPS), single-side-polished Si wafer (University Wafer, South Boston, MA) was used as substrates. These Si wafers were thoroughly cleaned via successive rinses, first with DI water, followed by acetone, and again with DI water before use. A quartz crystal microbalance (QCM; Maxtek, Inc., Cypress, CA) was used to investigate the mass increment per bilayer (BL). The crystal was rinsed between each deposition step and allowed to air-dry for stabilization, thereby minimizing the influence of water on the QCM mass measurements.

2.3. Film Deposition. PPy:NPs/DWNT-GO multilayer thin films were assembled by alternately immersing the substrates (Si wafers, PET, ITO, and quartz slide) onto oppositely charged PPy:NPs and DWNT-GO solutions by using a Multi Dip Coater robot (Hantech Co., Daejeon, South Korea). Briefly, each surface-treated substrate was dipped into a positively charged PPy:NP solution for 5 min, followed by three consecutive dip rinses in a DI water bath for 20 s each to eliminate any remaining physically adsorbed PPy:NPs. The PPy:NP-deposited sample was then immersed into the DWNT-GO suspension for 5 min and rinsed in the same manner to create a self-assembled PPy:NPs/DWNT-GO film. After completion of the first BL, an identical deposition cycle was employed, except that the deposition time was reduced from 5 to 1 min. The coating procedure was repeated until the desired number of layers was obtained.

2.4. Characterization. The film thickness was analyzed by using a NanoMap-PS stylus contact profiler (AEP Technology, Santa Clara, CA). Three measurements were conducted on each of the five samples, and the reported thickness represents an averaged value taken from a minimum of 15 separate measurements for each sample. To visualize the surface topography of the multilayer composites, AFM (Nanostation Surface Imaging Systems, Germany) was performed in the noncontact mode with a scanning rate of 1 Hz under ambient conditions. The top-surface structures of the thin films were observed via field-emission scanning electron microscopy (FE-SEM; S-4800, Hitachi, Japan). UV−vis spectroscopy of the thin films deposited on quartz slides was performed using a spectrophotometer (UV-1900, Shimadzu Corporation, Tokyo, Japan). To assess the ζ-potential of the PPy:NPs in solution, a nanoparticle size analyzer (Zetasizer Nano ZS90, Malvern Instruments Ltd., Worcestershire,

https://doi.org/10.1021/acsaem.3c03060
ACS Appl. Energy Mater. 2024, 7, 2351−2361

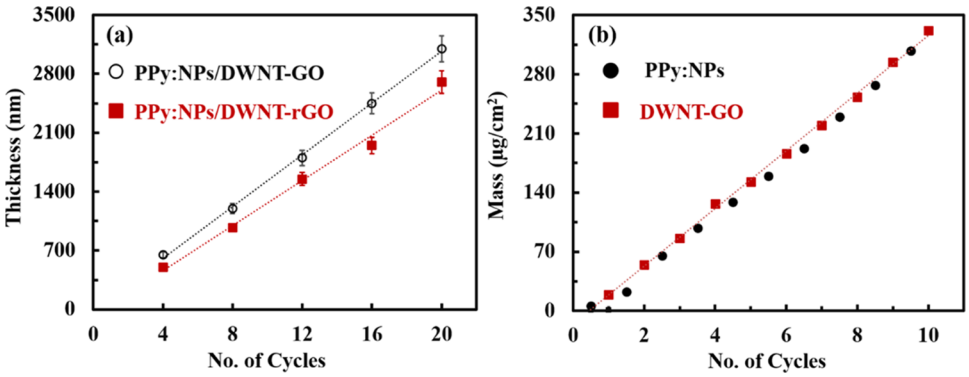

Figure 3. (a) Profilometer measured thickness on a silicon wafer before and after thermal reduction at 175 °C for 90 min and (b) mass of PPy:NPs/DWNT-GO LbL thin films as a function of bilayers deposited. Thermally reduced PPy:NPs/DWNT-GO systems are denoted as PPy:NPs/DWNT-rGO.

U.K.) with a 633 nm laser at a scattering angle of 13°, was used. The peak intensities of the PPy:NPs/DWNT-GO thin films, with and without thermal reduction, were acquired using XPS (Omicron NanoTechnology, Taunusstein, Germany) and Raman spectroscopy (DXR Raman microscope, ThermoFisher Scientific, Milan, Italy).

2.5. Thermoelectric Measurements. A standard four-point probe (CMT-100S, Advanced Instrument Technology) was used to measure the sheet resistances (R_s) of the LbL samples deposited on the PET substrates. Electrical conductivity (σ) was calculated as $\sigma = (R_s \cdot t)^{-1}$, where t is the thickness of the multilayer thin films. Before conducting the measurements, all of the samples were cut to the required dimensions (25 mm in length and 10 mm in width). The Seebeck coefficient was obtained with a four-point probe setup designed to measure electrical voltage ($\Delta V = V_{cold} - V_{hot}$) and temperature difference ($\Delta T = T_{hot} - T_{cold}$). Hall effect measurements were performed in the van der Pauw geometry (20 mm × 20 mm) at room temperature by using an Ecopia HMS-3000 measurement system (Ecopia, South Korea). To ensure repeatability and accuracy in determining carrier density, we conducted 20 separate measurements for each of these samples at three different currents (50, 100, and 150 μA) under a fixed magnetic field of 1 T. An X-ray photoelectron spectroscope (Sigma Probe, Thermo VG Scientific) was used to acquire UPS data from the LbL thin films deposited on the Au-coated Si wafers.

3. RESULTS AND DISCUSSION

Figure 2a,b depicts the PPy:NP/DWNT-GO assembly preparation process, including the chemical structures of each component. The formation of the multilayer composites is mainly driven by the strong electrostatic forces between the positively charged PPy:NPs and negatively charged GO. DWNT, stabilized in GO solutions, are presumably attached to the GO surface during deposition, primarily through interactions involving π stacking and van der Waals attraction.[46,47] In addition to the electrostatic forces, it is worth highlighting that hydrogen bonding between uncharged functional groups, such as carboxylic acid and hydroxyl groups, on GO sheets, likely reinforces the overall stability of the multilayer composites.[48] Due to its high water solubility, GO can function effectively as a dispersing agent for stabilizing carbon nanotubes (CNT) in a water-based environment.[49] This stabilization is achieved through the $\pi-\pi$ stacking interactions between the basal plane of the aromatic GO sheets and the surface of CNT.[50] Furthermore, the presence of oxygen-containing functional groups in GO helps to preserve the water stability of the CNT-GO complexes. Homogeneous black dispersions of PPy:NPs in water and DWNT suspensions in aqueous GO are shown in Figure 2c,d, respectively. Figure 2e shows an AFM image of the uniform distribution of the NPs in a dilute solution of positively charged PPy:NPs cast onto a Si wafer. These particles have a spherical shape, with diameters ranging from 160 to 200 nm, as evidenced by the SEM images (Figure 2f). The synthesized PPy:NPs exhibited a ζ-potential value of 25.5 ± 0.7 mV when measured using dynamic light scattering; this indicates that the NPs carry a positive charge in an aqueous solution. The uniformly distributed CNT structure and polymer-like entanglements of DWNT, evident in the AFM and SEM images (Figure 2g,h, respectively), highlight the stable nanotube suspensions in negatively charged GO. A 16-bilayer (BL) PPy:NPs/DWNT-GO thin film deposited on a PET substrate demonstrated excellent mechanical flexibility, allowing for easy bending, twisting, and rolling (Figure 2i).

3.1. Film Growth. Profilometry was used to investigate the growth behavior of the LbL thin films as a function of the number of BL deposited onto the Si wafers, as shown in Figure 3a. The PPy:NPs/DWNT-GO films exhibited linear growth as more layers were deposited, with each BL exhibiting an average thickness of 150 nm. Heat treatment of this system caused the multilayer thin films to shrink by 15% in thickness. GO is a single layer structure of graphene sheet and contains oxygen-rich functional groups, including carboxylic acid, ketone, and carbonyl groups, which are located at the edges of the sheet. Additionally, epoxide and hydroxyl groups are found on the basal plane of the GO in the form of hexagonal rings. Therefore, the slight reduction in the film thickness is likely attributable to the removal of oxygen functional groups attached to the GO surface via thermal treatment. The assembly of PPy:NPs/DWNT-GO thin films is presumably driven by a combination of factors. The ionic interactions between cationic PPy:NPs and anionic GO, along with hydrogen bonding, play a significant role. Additionally, strong $\pi-\pi$ interactions among PPy:NPs, DWNT, and GO may contribute to the assembly and networking of the multilayer composites. The mass increment, as measured by using a QCM, showed similar behavior to the thickness growth of the PPy:NPs/DWNT-GO films; this indicates that the composition remained constant throughout the assembly process (Figure 3b). This linear growth has been reported by other studies on LbL-based composites, wherein polyelectrolytes were incorporated with CNT and GO.[42,47] Although the mass increase of the multilayers has only been measured over 10 cycles, it is assumed to increase linearly up to 20 cycles, given the steadily increasing thickness observed.

https://doi.org/10.1021/acsaem.3c03060
ACS Appl. Energy Mater. 2024, 7, 2351−2361

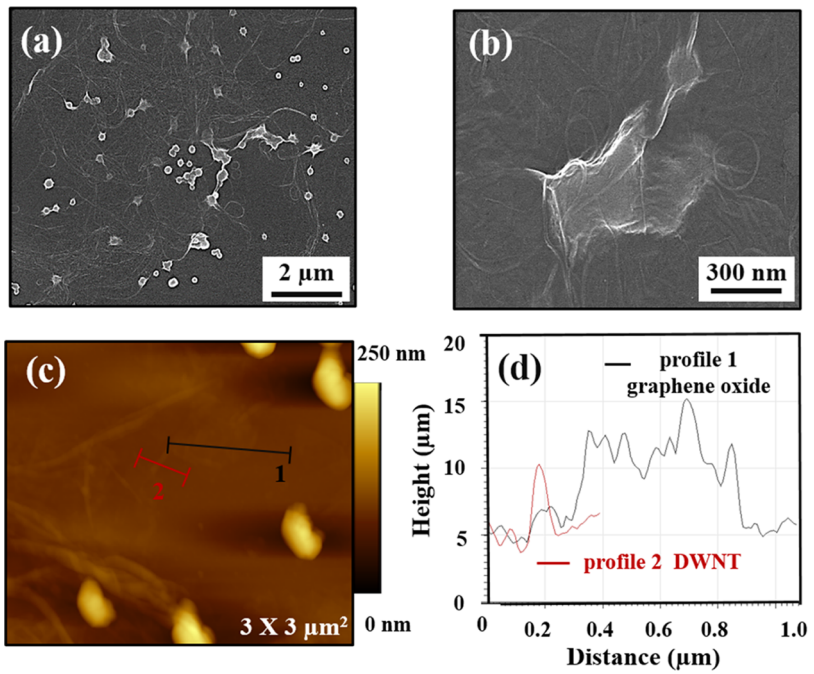

Figure 4. SEM images of (a) DWNT and PPy:NPs and (b) GO platelets and PPy nanoparticles surrounded by multiple nanotubes. AFM height images of (c) PPy:NPs, DWNT, and GO platelets uniformly coated on the 2-BL LbL thin films and (d) cross-sectional height profiles along the lines of graphene oxide (profile 1) and bundled carbon nanotubes (profile 2).

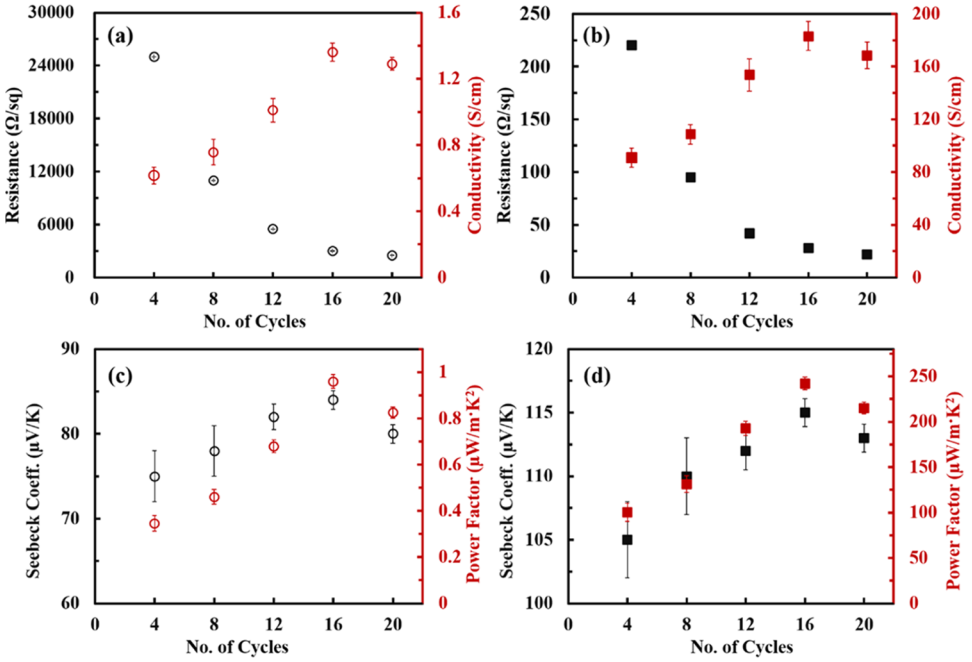

Figure 5. Thermoelectric properties of (a, c) PPy:NPs/DWNT-GO (open symbols) and (b, d) PPy:NPs/DWNT-rGO (closed symbols) as a function of bilayers deposited on PET substrates.

3.2. Surface Structure. The morphological surface structure of the PPy:NPs/DWNT-GO assemblies was examined via SEM and AFM (Figure 4). SEM images of the PPy:NPs/DWNT-GO multilayers exhibited multiple nanotubes and homogeneously dispersed PPy:NPs on the surface after a 2-BL coating on a Si wafer (Figure 4a). The SEM image in Figure 4b displayed that the interconnected DWNT bridges single GO platelets and PPy NPs, which is expected to enhance the electron conduction pathway throughout the multilayer structures. The surface of a 1-BL film showed spherical PPy:NPs lying on the DWNT surface (Figure S1a) and randomly oriented individual nanotubes and their bundles (Figure S1b). The top-surface image of the 2-BL PPy:NPs/DWNT-GO thin films revealed that a single GO plate and PPy:NPs were uniformly deposited, with multiple CNTs distributed across the surface (Figure 4c). A section analysis, obtained from a height image profile histogram, revealed that both the GO sheet and DWNT had thicknesses in the range

https://doi.org/10.1021/acsaem.3c03060
ACS Appl. Energy Mater. 2024, 7, 2351−2361

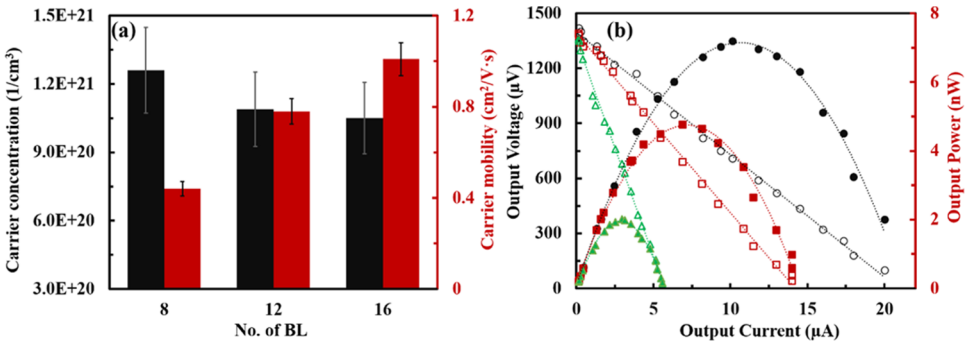

Figure 6. (a) Carrier concentration and carrier mobility of the PPy:NPs/DWNT-rGO films from Hall effect measurements. (b) Output voltage (open symbols) and output power (closed symbols) versus current of the PPy:NPs/DWNT-rGO films as a function of bilayers deposited (triangle, square, and circle indicate 8, 12, and 16-bilayer films, respectively).

3−5 nm (Figure 4d). This suggests that the nanotubes were fully exfoliated in the GO solutions and uniformly deposited in the multilayers during assembly. As the number of deposited BL increased, discerning the separate boundaries of the individual GO sheets in the stacked layers (Figure S2) became increasingly difficult (Figure S2). However, there was a noticeable entanglement of the nanotubes and PPy:NPs on the surface of the 20-BL PPy:NPs/DWNT-GO films. This indciates that the number of junctions between the PPy:NPs, DWNT, and GO increased with thickness, leading to the formation of a highly conjugated network. PPy:NPs/DWNT-GO systems after thermal reduction, hereafter referred to as PPy:NPs/DWNT-rGO films, exhibited very similar surface structures.

3.3. Thermoelectric Property. The TE performance of the LbL thin films deposited on an insulating PET substrate before and after the low-temperature treatment is shown in Figure 5. The sheet resistance of PPy:NPs/DWNT-GO thin films gradually decreased with the number of layers deposited (from 26 kΩ/sq at 4 BL to 3.2 kΩ/sq at 20-BL); this may be attributed to the increase in the connectivity of conductive components with thickness (Figure 5a). The electrical conductivity (σ), determined as the reciprocal of the product of the sheet resistance and film thickness, of this system was increased to a peak value of 1.36 S/cm at 16 BL and subsequently experienced a minor decline to 1.29 S/cm at 20-BL. As expected, a more significant improvement in the TE properties was observed in the PPy:NPs/DWNT-GO multilayers upon thermal reduction (Figure 5b). Thermal reduction at 175 °C converts GO to rGO. The reduction process for the multilayers coated on the 175 μm-thick PET substrates was gentle, ensuring that there was no observed loss or damage to the integrity of the film after thermal treatment. The σ values of PPy:NPs/DWNT-rGO films modestly increased with the number of layers (90.9 S/cm at 4 BL to 183.2 S/cm at 16 BL). This indicates that as more layers are deposited, a more interconnected network forms, facilitating electron transfer. Subsequently, σ leveled off at about 170 S/cm with further addition of layers beyond 16 BL, suggesting that the multilayer system is well above the percolation threshold with the formation of long-range connectivity.[51,52]

The Seebeck coefficient (S) as a function of the number of coating cycles on the PET substrates is shown in Figure 5c,d. The PPy:NPs/DWNT-GO films showed S values in the range of 75−84 μV/K. In PPy:NPs/DWNT-rGO films, the S value increased to a maximum of 115 μV/K at 16 BL and then plateaued after reaching 20-BL. This significant improvement in S observed in the thermally treated multilayer films is presumably because of the strong $\pi-\pi$ interfacial interaction between the PPy:NPs, DWNT, and rGO, which facilitates more efficient transport of charge carriers. As mentioned above, the PF value is determined as PF = $S^2\cdot\sigma$. The PPy:NPs/DWNT-GO composites showed an increase in PF from 0.35 μW/m·K^2 at 4 BL to 0.96 μW/m·K^2 at 16 BL. Remarkably, thermal treatment significantly enhances TE performances. Similarly to σ, the PF value of the PPy:NPs/DWNT-rGO films increased as the film thickness increased. The maximum PF of the PPy:NPs/DWNT-rGO films was 242.2 μW/m·K^2 at 16 BL, which is one of the highest values ever reported for PPy-based organic TE materials (Table S1).[53−56] TE properties of thermally reduced multilayer composites were studied at four different temperatures (120, 150, 175, and 200 °C). Both σ and S of the 16 BL PPy:NPs/DWNT-rGO films increased with the treatment temperature up to 175 °C. However, the effect of the treatment temperature was reduced at 200 °C, and each property was shown to be almost steady, as shown in Figures S3 and S4. This suggests that a uniform alignment of the three-dimensionally conjugated network structure is fully achieved during thermal reduction at 175 °C.d

Notably, a simultaneous increase in both σ and S was observed in these PPy:NPs/DWNT-rGO multilayers as more layers were added. This decoupled TE behavior is unusual in conventional bulk TE materials wherein S tends to decrease, and σ tends to increase with increasing carrier concentration (n).[15,57,58] To elucidate this simultaneous increase in TE behaviors, Hall Effect measurements were performed to analyze n and carrier mobility (μ), as shown in Figures 6a and S5. The n value of the thermally reduced 16 BL films increased by a factor of 5.1 compared to GO-based multilayers. Furthermore, the mobility of the PPy:NP/DWNT-rGO systems was 2 orders of magnitude higher than that of the untreated films. These significant increments in n and μ aid the high TE performance observed in the PPy:NP/DWNT-rGO after thermal reduction. The μ value of 16 BL PPy:NPs/DWNT-rGO more than doubled when the number of layers was increased from 8 to 16 BL. However, the n value decreased slightly from 1.26 × 10^{21} cm^{-3} at 8 BL to 1.05 × 10^{21} cm^{-3} at 16 BL. This indicates that the significant increase in μ leads to improved σ, whereas the decrease in n slightly enhances S. Practical application of these organic TE composites demands power generation, regardless of their theoretical ZT values. The open-circuit voltage (potential difference with no external load) and output power measurements of the PPy:NPs/DWNT-rGO films were analyzed, as shown in Figure 6b. Both

https://doi.org/10.1021/acsaem.3c03060
ACS Appl. Energy Mater. 2024, 7, 2351−2361

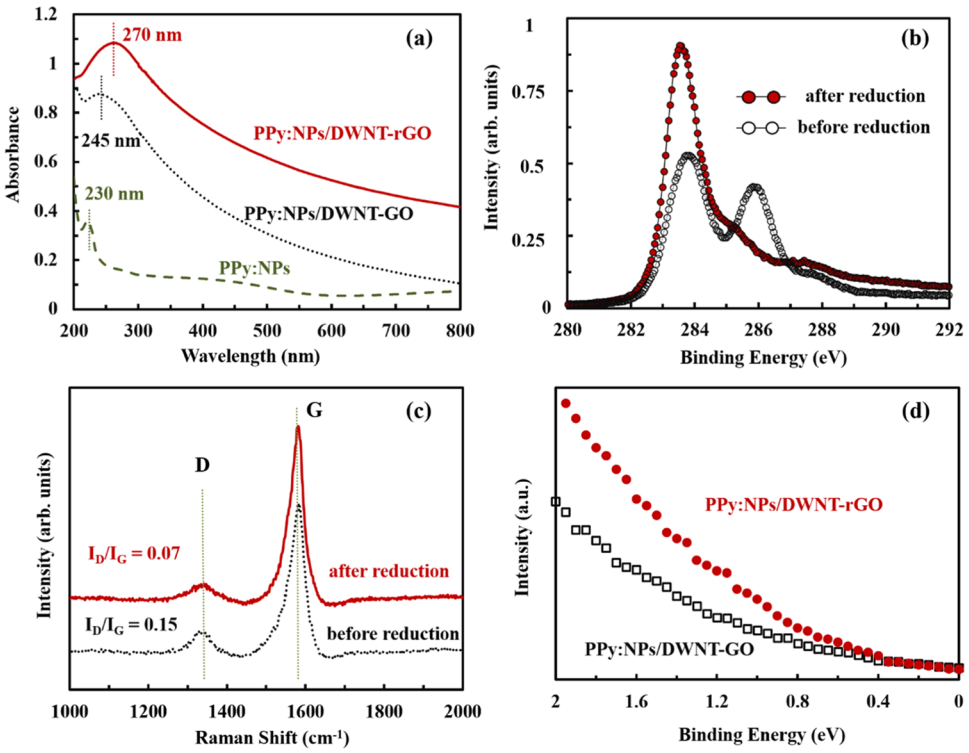

Figure 7. (a) UV−vis spectra of PPy:NPs and 3 BL PPy:NPs/DWNT-GO and PPy:NPs/DWNT-rGO films. (b) XPS, (c) Raman, and (d) UPS spectra of 20-BL PPy:NPs/DWNT-GO thin films before and after thermal reduction treatments.

the output voltage and TE power, measured from 8 to 16 BL, increased with more layers deposited. The maximum power generated from the 16 BL PPy:NPs/DWNT-rGO multilayer thin films was approximately 7.26 nW at for ΔT = 12.4 K.

3.4. Highly Tunable Thermoelectric Behavior. The superior TE properties of these PPy:NPs/DWNT-rGO multilayered composites can be explained by a synergistic interplay of three factors: (1) the intermolecular $\pi-\pi$ interactions in the multilayers, (2) an efficient transformation of GO to rGO through thermal reduction, and (3) the interconnected 3D structure formed by multiple layers composed of conjugated polymers and carbon nanofillers. The interfacial $\pi-\pi$ interactions among the components in the LbL films were confirmed by UV−vis spectroscopy. The strong absorption band at approximately 230 nm can be attributed to the conjugated bonds of the polypyrrole groups (the pyrrole ring $\pi-\pi^*$ electronic transitions).[59] After assembling into PPy:NPs/DWNT-GO multilayers, the adsorption peak was red-shifted to 245 nm, which is most likely due to the incorporation of conductive carbon nanofillers into the LbL films. The characteristic absorbance peak in the 3 BL PPy:NPs/DWNT-rGO films was further shifted to a higher wavelength by 25 nm, as compared to that of the respective films with no thermal reduction (Figure 7a). Such a red-shift implies that a low-temperature treatment strengthens the $\pi-\pi$ conjugation interaction between PPy:NPs and carbon nanofillers, consequently leading to an improved carrier mobility. This shift toward higher wavelength is directly associated with the extension of conjugation, which is primarily driven by the strong $\pi-\pi$ interaction between PPy:NPs and DWNT.[60] Moreover, the large surface area of the rGO could function as a conductive pathway to connect DWNT conducting domains, thereby leading to an improved percolation effect and a reduction in the energy barrier for electronic transitions. As a result, the enhanced charge delocalization of the carriers in the thermally reduced multilayer composites facilitates carrier transport within a 3D conjugated network.

GO platelets exhibit strong multiple interactions with PPy:NPs and DWNT within the multilayer structure and play a key role in creating a uniform dispersion of DWNT due to their anionic surface charge. However, the presence of oxygen functional groups in the GO can lead to electron scattering and may adversely affect carrier transport. This results in a reduction of the electrical conductivity in the PPy:NPs/DWNT-GO systems. The rehybridization of sp^3 to sp^2 carbon atoms after thermal reduction converts GO to rGO, dramatically enhancing the electrical conductivity (Figure 5a,b). The transport of charge carriers across the junctions between GO and DWNT in the PPy:NPs/DWNT-GO multilayers can be impeded due to the insulating properties of the GO layers. After thermal reduction, the Seebeck coefficient in the PPy:NPs/DWNT-rGO composites increased (Figure 5c,d). A significant improvement in the Seebeck coefficient may arise from the efficient carrier transport at the junctions between rGO and DWNT and can also be attributed to strong π electron interactions between PPy:NPs and rGO relative to untreated counterparts. XPS analysis further confirmed the deoxygenation of the GO sheets in the LbL assemblies, as shown in Figure 7b. The intensity of the C 1s peak at 286.2 eV, which is related to the oxygen functional groups, decreased relative to that appearing at 283.8 eV. This result suggests the removal of oxygen groups (e.g., C−OH, C−O−C, C═O, and −COOH) and restoration of the sp^2 C═C carbon bond network via thermal treatment.

To characterize the structural changes of GO in the composites that occur during a low-temperature treatment (i.e., conversion to the restored graphene structure), the molecular structures of the carbon products were analyzed by

https://doi.org/10.1021/acsaem.3c03060
ACS Appl. Energy Mater. 2024, 7, 2351−2361

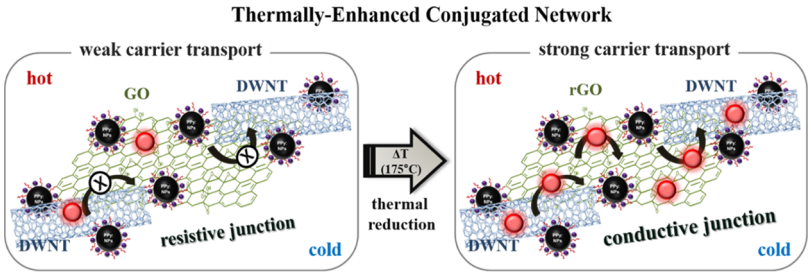

Figure 8. Schematic demonstration of carrier transport in PPy:NPs/DWNT-GO (left) and PPy:NPs/DWNT-rGO (right) thin films.

using Raman spectroscopy (Figure 7c). Both PPy:NPs/DWNT-GO and PPy:NPs/DWNT-rGO multilayers displayed two strong peaks at 1340 and 1580 cm^{-1}, each of which relates to the D (sp^3 vibration of carbon atoms due to the defects disordered structure of graphene surface and edges) and G bands (in-plane bond vibrations of sp^2-hybridized graphitic materials), respectively.[61] The ratio of the intensity of the D band to that of the G band (I_D/I_G) indicates disorder levels or structural defects in the graphene sheets. The I_D/I_G value for PPy:NPs/DWNT-rGO was lower relative to that of PPy:NPs/DWNT-GO, confirming that a more effective and expansive conjugated structure was generated via thermal reduction. The electronic structure of the multilayered composites was thoroughly analyzed using UPS results. Mott's formalism, $S(E, T) = \frac{\pi^2}{3}\cdot\frac{k^2T}{q}\cdot\left(\frac{\partial \ln(\sigma(E))}{\partial E}\right)_{E=E_f}$, suggests that the Seebeck coefficient exhibits a close correlation with the derivative of the density of states (DOS) at the Fermi level (E_f): the greater the Seebeck coefficient, the steeper would be the slope of DOS at E_f.[62] In other words, a steeper slope in the DOS at the Fermi level implies a more significant variation in available electronic states with energy, contributing to a larger Seebeck coefficient. The multilayer composites subjected to thermal reduction exhibited a steeper slope, suggesting that these LbL films had a larger Seebeck coefficient (Figure 7d). The highest molecular orbital (HOMO) and work function in both multilayer systems were determined on the basis of the UPS spectra (Table S2). The work function of the PPy:NPs/DWNT-rGO films was larger by 0.32 eV relative to that of the GO-based composites, indicating an upward shift of the HOMO edge. The larger energy difference between the HOMO and work function means that the Fermi level is positioned lower than the vacuum level. This is more favorable for p-type conversion, which in turn leads to an increase in the Seebeck coefficient.[63,64]

On the basis of the aforementioned results, carrier transport in the multilayers can be explained, as shown in Figure 8. GO-based multilayers are less conducive to electrical transport, which negatively impacts their TE performance (Figure 8, left). In comparison, the continuous 3D multilayer structure resulting from thermal reduction indicates the presence of a highly interconnected conjugation network, which facilitates efficient carrier transport and, thus, enhances the TE properties (Figure 8, right). The LbL self-assembly process, involving the nanoscaled layers with quasi-one-dimensional PPy:NPs, one-dimensional DWNT, and two-dimensional GO platelets in sequence, resulted in the formation of a highly interconnected 3D architectural structure that enhances carrier transport and TE properties. In this multilayered composite, the DWNT serves as a conductive bridge between the rGO sheets, creating an extended conjugated network that provides an effective pathway for carrier transport. This layered composite could also function as an energy filter due to the numerous interfaces created during LbL assembly, likely causing an energy-dependent scattering of the electrical carriers.[25] Energy filtering and energy potential barriers in the multilayered structures facilitate high-energy carriers to pass unimpeded under a temperature gradient while simultaneously scattering low-energy carriers at the junctions and in the layers above and below.[62,65] The cationically charged PPy:NPs are not only crucial for building up multilayer thin films but also vital in contributing to the conjugated network due to their intrinsically conductive properties. Although the electrical conductivity of PPy is much lower than that of the DWNT, it still contributes to the TE properties in the multilayers. Synergistic improvement occurs when positively charged PPy:NPs are connected by the bridges in PPy:NPs/DWNT-rGO, fully realizing the conductivity of the LbL films. This enhancement is achieved by incorporating PPy:NPs and carbonaceous nanofillers into a multilayer structure.

4. CONCLUSIONS

In this study, an LbL assembly process was employed to fabricate a novel organic TE composite through sequential deposition of positively charged water-soluble PPy:NPs and negatively charged DWNT-GO suspensions. The LbL-assembled composites exhibited uniform multilayer architectures with high homogeneity/orientation and well-defined layers, as confirmed by profiling, QCM measurements, AFM, and SEM. The TE performance of PPy:NPs/DWNT-GO thin films was significantly improved following low-temperature thermal treatments (175 °C for 90 min). A 16-bilayer PPy:NPs/DWNT-rGO thin film achieved remarkable electrical conductivity (183 S/cm) and Seebeck coefficient (115 μV/K), resulting in a high PF (242.2 $\mu W/m{\cdot}K^2$) at room temperature. This is among the highest power factors reported for PPy-based organic TE materials. The improved properties stem from the effective conversion of GO to rGO, creating a 3D network with strong π electron overlap between PPy:NPs and carbon nanofillers and enhancing carrier transport within the multilayers. The present work demonstrates a promising approach for enhancing the TE performance of layered composites of conductive polymers and carbon-based materials.

■ ASSOCIATED CONTENT

Supporting Information

The Supporting Information is available free of charge at https://pubs.acs.org/doi/10.1021/acsaem.3c03060.

SEM images of a one BL PPy:NPs/DWNT-GO LbL film, AFM image of the surface structure in 16 BL

https://doi.org/10.1021/acsaem.3c03060
ACS Appl. Energy Mater. 2024, 7, 2351−2361

PPy:NPs/DWNT-GO thin films, summarized table regarding electrical conductivity, Seebeck coefficient, and power factor of PPy-based organic composites, TE properties of 16 BL PPy:NPs/DWNT-rGO films as a function of thermal treatment temperature, carrier concentration and carrier mobility of 16 BL PPy:NPs/DWNT-GO and PPy:NPs/DWNT-rGO LbL thin films, and valence band edge (Ev) and work function measured on 16 BL LbL films before and after thermal reduction (PDF)

AUTHOR INFORMATION

Corresponding Authors

Mario Culebras − *Institute of Materials Science (ICMUV), University of Valencia, Paterna 46980, Spain*; Email: mario.culebras@uv.es

Jung Sang Cho − *Department of Engineering Chemistry, Chungbuk National University, Chungbuk 361-763, Republic of Korea*; Email: jscho@chungbuk.ac.kr

Chungyeon Cho − *Department of Carbon Convergence Engineering, College of Engineering, Wonkwang University, Iksan 54538, Republic of Korea*; orcid.org/0000-0001-6689-8106; Email: cncho37@wku.ac.kr

Authors

You-young Byun − *Department of Carbon Convergence Engineering, College of Engineering, Wonkwang University, Iksan 54538, Republic of Korea*

Junho Jang − *Wearable Platform Materials Technology Center (WMC), Department of Materials Science and Engineering, Korea Advanced Institute of Science and Technology (KAIST), Daejeon 34141, Republic of Korea*

Tae Kwon Lee − *Department of Environmental and Energy Engineering, Yonsei University, Wonju 26493, Republic of Korea*; orcid.org/0000-0003-3845-7316

Dongwhi Choi − *Department of Mechanical Engineering, Kyung Hee University, Gyeonggi-do 17104, Republic of Korea*; orcid.org/0000-0002-9286-2710

Aleksandra Serafin − *Stokes Laboratories, Bernal Institute, School of Engineering, University of Limerick, Limerick V94 T9PX, Ireland*; orcid.org/0000-0003-4285-6758

Maurice N. Collins − *Stokes Laboratories, Bernal Institute, School of Engineering, University of Limerick, Limerick V94 T9PX, Ireland*; orcid.org/0000-0003-2536-4508

Complete contact information is available at: https://pubs.acs.org/10.1021/acsaem.3c03060

Author Contributions

○M.C. and Y.-y.B. contributed equally to this study.

Notes

The authors declare no competing financial interest.

ACKNOWLEDGMENTS

This work was supported by the National Research Foundation of Korea (NRF) grant funded by the Korea Government (MSIT) (No. NRF-2021R1F1A1049361). M.C. thanks the Grant PID2021-124845OA-I00 funded by MCIN/AEI/10.13039/501100011033 and by the "European Union NextGenerationEU/PRTR."

REFERENCES

(1) Chong, Z. R.; Yang, S. H. B.; Babu, P.; Linga, P.; Li, X.-S. Review of Natural Gas Hydrates as an Energy Resource: Prospects and Challenges. *Appl. Energy* **2016**, *162*, 1633−1652.

(2) Rogdakis, K.; Karakostas, N.; Kymakis, E. Up-Scalable Emerging Energy Conversion Technologies Enabled by 2D Materials: from Miniature Power Harvesters Towards Grid-Connected Energy Systems. *Energy Environ. Sci.* **2021**, *14*, 3352−3392.

(3) Singh, P. K.; Kaur, G. A.; Shandilya, M.; Rana, P.; Rai, R.; Mishra, Y. K.; Syväjärvi, M.; Tiwari, A. Trends in Piezoelectric Nanomaterials Towards Green Energy Scavenging Nanodevices. *Mater. Today Sustainability* **2023**, *24*, No. 100583, DOI: 10.1016/j.mtsust.2023.100583.

(4) Wei, H.; Cui, D.; Ma, J.; Chu, L.; Zhao, X.; Song, H.; Liu, H.; Liu, T.; Wang, N.; Guo, Z. Energy Conversion Technologies Towards Self-Powered Electrochemical Energy Storage Systems: The State of the Art and Perspectives. *J. Mater. Chem. A* **2017**, *5*, 1873−1894.

(5) Yang, L.; Chen, Z. G.; Dargusch, M. S.; Zou, J. High Performance Thermoelectric Materials: Progress and Their Applications. *Adv. Energy Mater.* **2018**, *8*, No. 1701797.

(6) Blackburn, J. L.; Ferguson, A. J.; Cho, C.; Grunlan, J. C. Carbon-Nanotube-Based Thermoelectric Materials and Devices. *Adv. Mater.* **2018**, *30*, No. 1704386.

(7) Jia, Y.; Jiang, Q.; Sun, H.; Liu, P.; Hu, D.; Pei, Y.; Liu, W.; Crispin, X.; Fabiano, S.; Ma, Y.; Cao, Y. Wearable Thermoelectric Materials and Devices for Self-Powered Electronic Systems. *Adv. Mater.* **2021**, *33*, No. 2102990.

(8) Elsheikh, M. H.; Shnawah, D. A.; Sabri, M. F. M.; Said, S. B. M.; Hassan, M. H.; Bashir, M. B. A.; Mohamad, M. A Review on Thermoelectric Renewable Energy: Principle Parameters that Affect their Performance. *Renewable Sustainable Energy Rev.* **2014**, *30*, 337−355.

(9) Cho, C.; Wallace, K. L.; Tzeng, P.; Hsu, J. H.; Yu, C.; Grunlan, J. C. Outstanding Low Temperature Thermoelectric Power Factor from Completely Organic Thin Films Enabled by Multidimensional Conjugated Nanomaterials. *Adv. Energy Mater.* **2016**, *6*, No. 1502168.

(10) Wei, S.; Zhang, Y.; Lv, H.; Deng, L.; Chen, G. SWCNT Network Evolution of PEDOT: PSS/SWCNT Composites for Thermoelectric Application. *J. Chem. Eng.* **2022**, *428*, No. 131137.

(11) He, S.; Lehmann, S.; Bahrami, A.; Nielsch, K. Current State-of-the-Art in the Interface/Surface Modification of Thermoelectric Materials. *Adv. Energy Mater.* **2021**, *11*, No. 2101877.

(12) Bao, D.; Chen, J.; Yu, Y.; Liu, W.; Huang, L.; Han, G.; Tang, J.; Zhou, D.; Yang, L.; Chen, Z.-G. Texture-Dependent Thermoelectric Properties of Nano-Structured Bi_2Te_3. *J. Chem. Eng.* **2020**, *388*, No. 124295.

(13) Chen, B.; Das, S. R.; Zheng, W.; Zhu, B.; Xu, B.; Hong, S.; Sun, C.; Wang, X.; Wu, Y.; Claussen, J. C. Inkjet Printing of Single-Crystalline Bi_2Te_3 Thermoelectric Nanowire Networks. *Adv. Electron. Mater.* **2017**, *3*, No. 1600524.

(14) Pei, Y.; Lensch-Falk, J.; Toberer, E. S.; Medlin, D. L.; Snyder, G. J. High Thermoelectric Performance in PbTe due to Large Nanoscale Ag_2Te Precipitates and La Doping. *Adv. Funct. Mater.* **2011**, *21*, 241−249.

(15) Du, Y.; Xu, J.; Paul, B.; Eklund, P. Flexible Thermoelectric Materials and Devices. *Appl. Mater. Today* **2018**, *12*, 366−388.

(16) Gostkowska-Lekner, N.; Kojda, D.; Hoffmann, J.-E.; May, M.; Huber, P.; Habicht, K.; Hofmann, T. Synthesis of Organic−Inorganic Hybrids Based on the Conjugated Polymer P3HT and Mesoporous Silicon. *Microporous Mesoporous Mater.* **2022**, *343*, No. 112155.

(17) Goel, M.; Heinrich, C. D.; Krauss, G.; Thelakkat, M. Principles of Structural Design of Conjugated Polymers Showing Excellent Charge Transport Toward Thermoelectrics and Bioelectronics Applications. *Macromol. Rapid Commun.* **2019**, *40*, No. 1800915.

(18) Ding, L.; Yu, Z.-D.; Wang, X.-Y.; Yao, Z.-F.; Lu, Y.; Yang, C.-Y.; Wang, J.-Y.; Pei, J. Polymer Semiconductors: Synthesis, Processing, and Applications. *Chem. Rev.* **2023**, *123*, 7241−7497.

(19) Yan, H.; Ohno, N.; Toshima, N. Low Thermal Conductivities of Undoped and Various Protonic Acid-Doped Polyaniline Films. *Chem. Lett.* **2000**, *29*, 392−393.
(20) Toshima, N.; Ichikawa, S. Conducting Polymers and Their Hybrids as Organic Thermoelectric Materials. *J. Electron. Mater.* **2015**, *44*, 384−390.
(21) Wang, Y.; Yang, L.; Shi, X. L.; Shi, X.; Chen, L.; Dargusch, M. S.; Zou, J.; Chen, Z. G. Flexible Thermoelectric Materials and Generators: Challenges and Innovations. *Adv. Mater.* **2019**, *31*, No. 1807916.
(22) Sun, F.; Jiang, H.; Wang, H.; Zhong, Y.; Xu, Y.; Xing, Y.; Yu, M.; Feng, L.-W.; Tang, Z.; Liu, J.; et al. Soft Fiber Electronics Based on Semiconducting Polymer. *Chem. Rev.* **2023**, *123*, 4693−4763.
(23) Freer, R.; Powell, A. V. Realising the Potential of Thermoelectric Technology: A Roadmap. *J. Mater. Chem. C* **2020**, *8*, 441−463.
(24) Eryilmaz, I. H.; Chen, Y.-F.; Mattana, G.; Orgiu, E. Organic Thermoelectric Generators: Working Principles, Materials, and Fabrication Techniques. *Chem. Commun.* **2023**, *59*, 3160−3174.
(25) Nandihalli, N.; Liu, C.-J.; Mori, T. Polymer Based Thermoelectric Nanocomposite Materials and Devices: Fabrication and Characteristics. *Nano Energy* **2020**, *78*, No. 105186.
(26) Zhang, Y.; Zhang, Q.; Chen, G. Carbon and Carbon Composites for Thermoelectric Applications. *Carbon Energy* **2020**, *2*, 408−436.
(27) Culebras, M.; Choi, K.; Cho, C. Recent Progress in Flexible Organic Thermoelectrics. *Micromachines* **2018**, *9*, 638.
(28) Yang, Y.; Deng, H.; Fu, Q. Recent progress on PEDOT: PSS Based Polymer Blends and Composites for Flexible Electronics and Thermoelectric Devices. *Mater. Chem. Front.* **2020**, *4*, 3130−3152.
(29) Zhao, S.; Caruso, F.; Dähne, L.; Decher, G.; De Geest, B. G.; Fan, J.; Feliu, N.; Gogotsi, Y.; Hammond, P. T.; Hersam, M. C.; et al. The Future of Layer-By-Layer Assembly: a Tribute to ACS Nano Associate Editor Helmuth Mohwald. *ACS Nano* **2019**, *13*, 6151−6169.
(30) Mariani, S.; Robbiano, V.; Strambini, L. M.; Debrassi, A.; Egri, G.; Dähne, L.; Barillaro, G. Layer-By-Layer Biofunctionalization of Nanostructured Porous Silicon for High-Sensitivity and High-Selectivity Label-Free Affinity Biosensing. *Nat. Commun.* **2018**, *9*, No. 5256.
(31) Richardson, J. J.; Cui, J.; Bjornmalm, M.; Braunger, J. A.; Ejima, H.; Caruso, F. Innovation in Layer-By-Layer Assembly. *Chem. Rev.* **2016**, *116*, 14828−14867.
(32) Borges, J.; Mano, J. F. Molecular Interactions Driving the Layer-By-Layer Assembly of Multilayers. *Chem. Rev.* **2014**, *114*, 8883−8942.
(33) Richardson, J. J.; Björnmalm, M.; Caruso, F. Technology-Driven Layer-By-Layer Assembly of Nanofilms. *Science* **2015**, *348*, No. aaa2491.
(34) Gentile, P.; Carmagnola, I.; Nardo, T.; Chiono, V. Layer-by-Layer Assembly for Biomedical Applications in the Last Decade. *Nanotechnology* **2015**, *26*, No. 422001.
(35) Zhu, X.; Loh, X. J. Layer-By-Layer Assemblies for Antibacterial Applications. *Biomater. Sci.* **2015**, *3*, 1505−1518.
(36) Zhang, S.; Xia, F.; Demoustier-Champagne, S.; Jonas, A. M. Layer-By-Layer Assembly in Nanochannels: Assembly Mechanism and Applications. *Nanoscale* **2021**, *13*, 7471−7497.
(37) Yuan, W.; Weng, G.-M.; Lipton, J.; Li, C. M.; Van Tassel, P. R.; Taylor, A. D. Weak Polyelectrolyte-Based Multilayers Via Layer-By-Layer Assembly: Approaches, Properties, and Applications. *Adv. Colloid Interface Sci.* **2020**, *282*, No. 102200.
(38) Choi, I.; Suntivich, R.; Plamper, F. A.; Synatschke, C. V.; Müller, A. H.; Tsukruk, V. V. pH-Controlled Exponential and Linear Growing Modes of Layer-By-Layer Assemblies of Star Polyelectrolytes. *J. Am. Chem. Soc.* **2011**, *133*, 9592−9606.
(39) Cho, C.; Culebras, M.; Wallace, K. L.; Song, Y.; Holder, K.; Hsu, J.-H.; Yu, C.; Grunlan, J. C. Stable N-Type Thermoelectric Multilayer Thin Films with High Power Factor From Carbonaceous Nanofillers. *Nano Energy* **2016**, *28*, 426−432.
(40) Parbat, D.; Jana, N.; Dhar, M.; Manna, U. Reactive Multilayer Coating As Versatile Nanoarchitectonics for Customizing Various Bioinspired Liquid Wettabilities. *ACS Appl. Mater. Interfaces* **2023**, *15*, 25232−25247.
(41) Byun, Y.-y.; Jang, J.; Culebras, M.; Bae, B.-S.; Cho, J. S.; Park, Y. T.; Cho, C. Conformation-Dependent Thermoelectric Power Factor of Multilayer Nanocomposites. *Appl. Surf. Sci.* **2022**, *594*, No. 153483.
(42) Cho, C.; Stevens, B.; Hsu, J. H.; Bureau, R.; Hagen, D. A.; Regev, O.; Yu, C.; Grunlan, J. C. Completely Organic Multilayer Thin Film with Thermoelectric Power Factor Rivaling Inorganic Tellurides. *Adv. Mater.* **2015**, *27*, 2996−3001.
(43) Shu, Y.; Xiong, Z.; Liu, Y.; Zhou, Y.; Li, M.; Zheng, Y.; Chen, S.; Sun, K.Thermoelectric Properties of Carbon Nanomaterials/Polymer Composites. In *Flexible Thermoelectric Polymers and Systems*; Wiley, 2022; pp 163−207.
(44) Cho, C.; Song, Y.; Hsu, J.-H.; Yu, C.; Stevens, D. L.; Grunlan, J. C. Organic Thermoelectric Thin Films with Large P-Type and N-Type Power Factor. *J. Mater. Sci.* **2021**, *56*, 4291−4304.
(45) Sun, Y.; Di, C. A.; Xu, W.; Zhu, D. Advances in N-Type Organic Thermoelectric Materials and Devices. *Adv. Electron. Mater.* **2019**, *5*, No. 1800825.
(46) Liang, X.; Cheng, Q. Synergistic Reinforcing Effect from Graphene and Carbon Nanotubes. *Compos. Commun.* **2018**, *10*, 122−128.
(47) Cho, C.; Bittner, N.; Choi, W.; Hsu, J. H.; Yu, C.; Grunlan, J. C. Thermally Enhanced N-Type Thermoelectric Behavior in Completely Organic Graphene Oxide-Based Thin Films. *Adv. Electron. Mater.* **2019**, *5*, No. 1800465.
(48) Choi, W.; Choi, J.; Bang, J.; Lee, J.-H. Layer-By-Layer Assembly of Graphene Oxide Nanosheets on Polyamide Membranes for Durable Reverse-Osmosis Applications. *ACS Appl. Mater. Interfaces* **2013**, *5*, 12510−12519.
(49) Zhang, C.; Ren, L.; Wang, X.; Liu, T. Graphene Oxide-Assisted Dispersion of Pristine Multiwalled Carbon Nanotubes in Aqueous Media. *J. Phys. Chem. C* **2010**, *114*, 11435−11440.
(50) Cho, C.; Qin, S.; Choi, K.; Grunlan, J. C. Improved Thermoelectric Power Factor in Completely Organic Nanocomposite Enabled by L-Ascorbic Acid. *ACS Appl. Polym. Mater.* **2019**, *1*, 1942−1947.
(51) Song, Y.; Kim, D.; Kang, S.; Ko, Y.; Ko, J.; Huh, J.; Ko, Y.; Lee, S. W.; Cho, J. Room-Temperature Metallic Fusion-Induced Layer-By-Layer Assembly for Highly Flexible Electrode Applications. *Adv. Funct. Mater.* **2019**, *29*, No. 1806584.
(52) Liu, H.; Li, Y.; Dai, K.; Zheng, G.; Liu, C.; Shen, C.; Yan, X.; Guo, J.; Guo, Z. Electrically Conductive Thermoplastic Elastomer Nanocomposites at Ultralow Graphene Loading Levels for Strain Sensor Applications. *J. Mater. Chem. C* **2016**, *4*, 157−166.
(53) Song, H.; Cai, K.; Wang, J.; Shen, S. Influence of Polymerization Method on the Thermoelectric Properties of Multi-Walled Carbon Nanotubes/Polypyrrole Composites. *Synth. Met.* **2016**, *211*, 58−65.
(54) Xiang, M.; Yang, Z.; Chen, J.; Zhou, S.; Wei, W.; Dong, S. Polymeric Thermoelectric Composites by Polypyrrole and Cheap Reduced Graphene Oxide in Towel-Gourd Sponge Fibers. *ACS Omega* **2020**, *5*, 29955−29962.
(55) Fan, W.; Zhang, Y.; Guo, C.-Y.; Chen, G. Toward High Thermoelectric Performance for Polypyrrole Composites by Dynamic 3-Phase Interfacial Electropolymerization and Chemical Doping of Carbon Nanotubes. *Compos. Sci. Technol.* **2019**, *183*, No. 107794.
(56) Wang, Y.; Yang, J.; Wang, L.; Du, K.; Yin, Q.; Yin, Q. Polypyrrole/Graphene/Polyaniline Ternary Nanocomposite with High Thermoelectric Power Factor. *ACS Appl. Mater. Interfaces* **2017**, *9*, 20124−20131.
(57) Wang, S.; Chang, C.; Bai, S.; Qin, B.; Zhu, Y.; Zhan, S.; Zheng, J.; Tang, S.; Zhao, L.-D. Fine Tuning of Defects Enables High Carrier Mobility and Enhanced Thermoelectric Performance of N-Type PbTe. *Chem. Mater.* **2023**, *35*, 755−763.

https://doi.org/10.1021/acsaem.3c03060
ACS Appl. Energy Mater. 2024, 7, 2351−2361

(58) Tan, G.; Zhao, L.-D.; Kanatzidis, M. G. Rationally Designing High-Performance Bulk Thermoelectric Materials. *Chem. Rev.* **2016**, *116*, 12123−12149.
(59) Shrestha, B. K.; Ahmad, R.; Shrestha, S.; Park, C. H.; Kim, C. S. Globular Shaped Polypyrrole Doped Well-Dispersed Functionalized Multiwall Carbon Nanotubes/Nafion Composite for Enzymatic Glucose Biosensor Application. *Sci. Rep.* **2017**, *7*, No. 16191.
(60) Bachhav, S. G.; Patil, D. R. Study of Polypyrrole-Coated MWCNT Nanocomposites for Ammonia Sensing at Room Temperature. *J. Mater. Sci. Chem. Eng.* **2015**, *03*, 30.
(61) Ferrari, A. C.; Robertson, J. Interpretation of Raman Spectra of Disordered and Amorphous Carbon. *Phys. Rev. B* **2000**, *61*, 14095.
(62) Yao, J.-A.; Peng, X.-X.; Liu, Z.-K.; Zhang, Y.-F.; Fu, P.; Li, H.; Lin, Z.-D.; Du, F.-P. Enhanced Thermoelectric Properties of Bilayer-Like Structural Graphene Quantum Dots/Single-Walled Carbon Nanotubes Hybrids. *ACS Appl. Mater. Interfaces* **2020**, *12*, 39145−39153.
(63) Stevens, D. L.; Parra, A.; Grunlan, J. C. Thermoelectric Performance Improvement of Polymer Nanocomposites by Selective Thermal Degradation. *ACS Appl. Energy Mater.* **2019**, *2*, 5975−5982.
(64) Kim, S. L.; Choi, K.; Tazebay, A.; Yu, C. Flexible Power Fabrics Made of Carbon Nanotubes for Harvesting Thermoelectricity. *ACS Nano* **2014**, *8*, 2377−2386.
(65) Wang, Y.; Bai, Z.; Guo, Y.; Liu, C.; Jiang, Q.; Jiang, F.; Yang, J.; Ding, W.; Liu, P.; Xu, J. Recent Advances in 2D Material/Conducting Polymer Composites for Thermoelectric Energy Conversion. *Macromol. Mater. Eng.* **2022**, *307*, No. 2200107.

https://doi.org/10.1021/acsaem.3c03060
ACS Appl. Energy Mater. 2024, 7, 2351−2361